Gut microbial interaction networks control autoimmunity to neuroretina

Amy Zhang[1#], Reiko Horai[1#*], Yingyos Jittayasothorn[1], Jonathan H. Badger[2], Zhichao Wu[3], Guangpu Shi[1], Akriti Gupta[1], Samyuktha Arunkumar[1], Caitlin E. Murphy[1], Vijayaraj Nagarajan[1], John A. McCulloch[2], Shilpa Kodati[1], H Nida Sen[1], Jung Wha Lee[1], Jonathan P. Jacobs[4], Xiaoyan Xu[1], Mary J. Mattapallil[1], Zixuan Peng[1], Biying Xu[1], Robert J. Palmer[5], Nadim Majdalani[6], Kenya Honda[7], Colm O'hUigin[2], Rachel R. Caspi[1*]

[1]Laboratory of Immunology, National Eye Institute, National Institutes of Health, Bethesda, MD, USA

[2]Genetics and Microbiome Core, Laboratory of Integrative Cancer Immunology, Center for Cancer Research, National Cancer Institute, National Institutes of Health, Bethesda, MD, USA

[3]Laboratory of Pathology, Center for Cancer Research, National Cancer Institute, National Institutes of Health, Bethesda, MD, USA

[4]Goodman-Luskin Microbiome Center, David Geffen School of Medicine at UCLA, Los Angeles, CA, USA

[5]Structural Biochemistry Unit, National Institute of Dental and Craniofacial Research, National Institutes of Health, Bethesda, MD, USA

[6]Laboratory of Molecular Biology, Center for Cancer Research, National Cancer Institute, National Institutes of Health, Bethesda, MD, USA

[7]Keio University School of Medicine, Tokyo, Japan

[#]Equal contribution

*Correspondence to:

Rachel R. Caspi (caspir@nei.nih.gov)

Laboratory of Immunology, National Eye Institute, National Institutes of Health
10 Center Drive, 10/10N248, Bethesda, MD 20892-1857, USA

Reiko Horai (hreiko@nih.gov)

Laboratory of Immunology, National Eye Institute, National Institutes of Health
10 Center Drive, 10/10S243, Bethesda, MD 20892-1857, USA

Running title: Gut microbial interactions drive autoimmune uveitis

Funding: NIH/NEI Intramural funding, Project Number EY000184

Commercial Disclosures: None

KEYWORDS

Gut microbiome, Autoimmune uveitis, Akkermansia, Short-chain fatty acids, Th1 effector response, human flora

ABSTRACT

The gut microbiome influences the development of immune-mediated inflammatory diseases, including autoimmune uveitis, a sight-threatening ocular inflammation driven by retina-specific T cells[1]. Using a model of spontaneous autoimmune uveitis (sEAU) we showed that gut commensals provide immune stimuli that trigger disease[2]. Here we report that uveitis-promoting microbes are present in human gut flora and that colonization of germ-free (GF) mice with commensals from healthy human donors was sufficient to provoke disease. Severity of sEAU correlated with expansion of Akkermansia and contraction of short-chain fatty acid (SCFA)–producing Firmicutes, followed by decreased SCFA levels and a dominant gut Th1 effector response. Mechanistic gain-of-function experiments, enriching GF sEAU mice with Akkermansia, reproduced these microbiome, metabolite and immune phenotype shifts, and exacerbated disease, suggesting that Akkermansia promotes autoimmunity by outcompeting SCFA-producers and enhancing Th1-type responses. An inverse correlation between Akkermansia (Verrucomicrobia) and Firmicutes was also present in patients with uveitis, multiple sclerosis and Crohn's disease. These findings reveal a stereotypic gut microbial interaction network that regulates systemic immune balance, and may represent an ecologically conserved mechanism through which the gut microbiome modulates autoimmune and inflammatory diseases.

INTRODUCTION

Immune-privileged tissues are increasingly recognized as sites where host–microbiota interactions influence immunological balance in autoimmune and inflammatory diseases[3,4]. Multiple mechanisms have been proposed that explain the central role of microbiota in driving inflammation in the central nervous system (CNS), including innate and adaptive effects such as molecular mimicry[2,5], bystander activation[6], epitope spreading[7,8] and dual T cell receptors (TCRs)[9]. The eye, especially the neuroretina, is part of the CNS and represents a quintessential immune-privileged tissue, making it a valuable model to study immune privilege and autoimmunity in the CNS.

Autoimmune uveitis is a T cell-driven intraocular inflammation of unknown etiology that targets the neuroretina and can lead to blindness[1]. It is represented by the models of experimental autoimmune uveitis (EAU) in animals. EAU is induced in wild type mice by immunization with the retinal antigen IRBP[1], or can develop spontaneously (sEAU) in mice expressing a transgenic IRBP-specific TCR cloned from the immunization induced model (line R161H)[10]. Our previous studies highlighted the critical role of gut microbiome in triggering sEAU by providing antigenic stimuli that activate retina-specific T cells[2]. Subsequent research reported inhibitory effects of microbiome depletion also in induced EAU[11], where the antigen is provided, emphasizing the antigen-independent (innate?) effects of gut microbes on EAU. Interestingly, gut microbiome studies in uveitis patients have revealed differences in gut flora between patients and healthy controls[12-16], but mechanistic information could not be resolved.

Because inductive events and causal relationships cannot be studied in patients, we employed the model of sEAU in R161H TCR transgenic mice[10], which may provide a more physiological system to study triggers delivered by the microbiota. To gain mechanistic insights into how human gut microbiota might affect the development of autoimmune uveitis, we created gnotobiotic breeding colonies of R161H mice harboring healthy human gut flora by reconstituting GF parental mice with fecal material from three healthy human donors. The rationale for focusing on healthy donors is that *(i)* every uveitis patient was once a healthy person, so by definition, uveitis-relevant microbes should be present in the healthy person's gut flora, and *(ii)* the composition of patient

flora could have been altered by their disease or by their treatment, confounding data interpretation.

Using a multiomic strategy that integrates microbial, metabolomic and immune profiling of human flora (HuFl)-reconstituted R161H mice, combined with analyses of human autoimmune disease datasets, we identified a microbial interaction network comprising an “Akkermansia/Verrucomicrobia—Firmicutes axis” that appears to regulate autoimmunity. Our data points to an underexplored but fundamental mechanism, where interactive relationships in the microbial community play a central role in regulation of autoimmune disease pathogenesis by microbiota[17].

RESULTS

1. Human gut commensals support development of spontaneous experimental autoimmune uveitis (sEAU)

R161H mice harboring mouse microbiota (specific-pathogen-free, SPF) typically develop moderate to severe uveitis with high penetrance (100% incidence by two months of age)[10]. To first assess whether human gut microbiota affect uveitis development, we developed “humanized gnotobiotic” R161H mouse lines as our pre-clinical model, by reconstituting breeding pairs of GF R161H mice with gut microbiota from three healthy human subjects—U, V, and W. Each line was maintained in separate isolators through successive generations, so that the offspring acquired the human flora naturally from their respective parents (Fig. 1a).

Microbiome sequencing results showed successful engraftment of human flora in gnotobiotic R161H mice. The succession of gut microbiota through generations of breeding in gnotobiotic isolators did not appear to diminish the differences between individual cohorts, and each U, V, or W mouse recipient cohort preserved the microbial signatures of its original donor (Fig. 1b).

57 Human commensal microbes supported uveitis development in R161H mice. Although
58 HuFI mice display a broad spectrum of disease scores, the scores were on average lower
59 than those of SPF mice that harbor normal mouse flora (Fig. 1c & Extended Data Fig.
60 1a). We did not observe obvious sex differences with respect to disease severity in HuFI
61 mice (Extended Data Fig. 1b). Immune phenotype of colonic $CD4^+$ T cells, based on a
62 range of cell surface and intracellular markers, clearly distinguished HuFI mice from GF
63 and SPF mice (Fig 1d & Extended Data Fig. 1c-e). The HuFI mice showed a spectrum of
64 disease scores and memory marker expression between GF (low) and SPF (high) mice
65 (Fig. 1e), had fewer IFN-γ-producing Th1 and IL-17A-producing Th17 effector cells and
66 more regulatory T cells (Tregs) expressing Foxp3 and IL-10 than did SPF mice (Fig. 1f-
67 g). This immune phenotype was consistent with other activation markers and Th1/Th17
68 signature molecules (Extended Data Fig. 1e). This phenotype may explain the lower
69 disease scores that they developed.

70 **2. HuFI sEAU tracks with a dominant Th1 phenotype and abundance of**
71 **Verrucomicrobia/Akkermansia**

72 Since both Th1 and Th17 effector phenotypes can drive autoimmune uveitis[18-20], we set
73 out to define the immune signatures that associate with disease in the HuFI model. We
74 categorized histological scores into high (score ≥ 1.5), mid (0.75 < score < 1.5), and low
75 (score ≤ 0.75) to facilitate statistical analysis. Interestingly, IFN-γ-producing CD4 T cells,
76 rather than IL-17A producers, in the gut (and other tissues) associated strongly with
77 severe disease phenotype (Fig. 2a-d). This suggests that uveitis development in HuFI
78 mice is more dependent on Th1 than Th17.

79 Microbiome analysis of parental and offspring HuFI mice showed that colonized mice
80 adopted only a subset of the original donor taxa (Extended Data Fig. 2a-b). This could be
81 a result from loss during human stool sample preservation and transfer processes, and/or
82 from inefficient engraftment of some non-native microbes to the gut environment of a
83 different host species. However, in terms of the overall microbial composition, each
84 mouse cohort remained closer to their original donor, preserving a distinct microbial
85 footprint (Fig. 1b & Extended Data Fig. 2c-d). Differences between female *vs.* male HuFI
86 mice in terms of microbial abundance and composition were minimal, if any, compared to

87 the differences based on human donors (Extended Data Fig. 2e-f). This is compatible
88 with the apparent lack of sex differences in disease severity of HuFI mice (Extended Data
89 Fig. 1b).

90 We then explored how gut microbiome associates with severity of uveitis. Correlational
91 heat map of major bacterial taxa at the family level revealed strong links between several
92 taxa and histology scores (Fig. 2e). Among them, Akkermansia (the only representative
93 of Verrucomicrobia in HuFI mice) correlated with high disease scores (Pearson $r = 0.5$,
94 FDR <0.05), whereas certain members of the Firmicutes phylum were correlated with low
95 disease scores (Pearson $r = -0.3$, FDR <0.05). Differential abundance analysis between
96 high and low histology categories consistently showed that Akkermansia was enriched in
97 mice with high disease, whereas Firmicutes (especially Clostridia) were enriched in mice
98 with low disease (Fig. 2f-g & Extended Data Fig. 2g).

99 **3. SCFA signatures are enriched in low disease HuFI mice or healthy subjects**

100 SCFAs are metabolites of commensal gut microbes resulting from fermentation of dietary
101 fiber, and have anti-inflammatory properties in a range of pathological conditions[21]. Some
102 SCFAs, e.g. butyrate and propionate, may have therapeutic potential in induced EAU[22,23].
103 In the current study, a key observation from differential abundance analyses of mice with
104 low and high disease scores was that SCFA-producing Firmicutes were associated with
105 lower sEAU scores (Fig. 2e). Therefore, it appeared plausible that SCFAs may also have
106 the potential to modulate sEAU.

107 To address this, we mined functional gene signatures from shotgun metagenomic
108 sequences of HuFI mice. Genes known to be involved in SCFAs synthesis and
109 metabolism were mapped to the simplified pathways shown in Fig. 3a. Consistent with
110 the observed differences in microbial abundance (Fig. 2e), the genes involved in main
111 SCFA pathways were enriched in mice with low disease scores and reduced in mice with
112 high disease scores (Fig. 3b). In agreement with the pathway analysis, metabolomic
113 quantification of SCFAs in the gut and serum of the mice confirmed that higher disease
114 scores were associated with lower SCFA concentrations both locally and systemically
115 (Fig. 3c).

116 We next examined whether this signature was present in a cohort of uveitis patients seen
117 at the National Eye Institute (NEI) clinic, compared to healthy controls. Because uveitis is
118 a heterogenous disease, we focused on a subset of patients whose disease was
119 restricted to the eye (idiopathic uveitis, Vogt-Koyanagi-Harada disease/sympathetic
120 ophthalmia and birdshot chorioretinopathy), as modeled by EAU, rather than being part of
121 a systemic syndrome. Similarly to the HuFI R161H mice, enzymes involved in acetate,
122 butyrate and propionate pathways (Fig. 3d) and their corresponding SCFAs (Fig. 3e),
123 were reduced in uveitis patients compared to healthy controls. This supports a role for
124 SCFAs in regulation of human uveitis.

125 **4. Akkermansia negatively correlates with Firmicutes in both sEAU and clinical**
126 **uveitis**

127 Among all taxa in HuFI mice, Akkermansia abundance was shown to be a prominent
128 correlate of severe uveitis and IFN-γ-producing CD4+ T cells in the gut (Fig. 2e-f,
129 Extended Data Fig. 3a–b), whereas SCFA-producing Firmicutes were reduced in the
130 same animals (Fig. 2e, g). We therefore analyzed their relative abundance and potential
131 interdependence to determine whether competitive interactions between these taxa might
132 contribute to autoimmune uveitis.

133 We first quantified abundance of Akkermansia and Firmicutes, and found them to be
134 inversely correlated (Fig. 4a). An in-depth computational analysis of the bacterial
135 association network confirmed the negative correlation between Akkermansia and
136 multiple families of SCFA-producing Firmicutes (Fig. 4b, Extended Data Fig. 3c). Levels
137 of major SCFAs in feces also exhibited an inverse correlation with Akkermansia
138 abundance (Fig. 4c). Taken together, this supports an interpretation of a negative
139 interaction between Akkermansia and a range of SCFA-producing microbes.

140 Similarly, gut microbiome interaction networks of uveitis patients displayed a negative
141 relationship between Verrucomicrobia (primarily Akkermansia) and SCFA-producing
142 Firmicutes (Clostridia, class level), but this relationship was not evident in healthy
143 subjects (Fig. 4d). This supports the relevance of the sEAU model to clinical disease.

144 **5. Akkermansia promotes uveitis by outcompeting SCFA producers and**
145 **decreasing circulating SCFA levels**

146 To validate the proposed microbiome interaction network *in vivo*, we used a gain-of-
147 function approach, where GF R161H mice received Akkermansia alone or Akkermansia
148 mixed with HuFI mouse donor fecal flora. In the first paradigm, we associated GF mice *de*
149 *novo* with cultured *Akkermansia muciniphila* (the type species of Akkermansia) or with
150 sterile PBS as control, and maintained them in static microisolators using sterile handling
151 techniques, to minimize additional microbial exposure (Extended Data Fig. 4a). This
152 approach resulted in a minimal gut microbial population of very low diversity (≤10 total
153 detectable taxa/mouse), dominated by Verrucomicrobia (Akkermansia) and Firmicutes
154 (Extended Data Fig. 4b-d).

155 First paradigm: A single oral gavage led to successful and sustained engraftment of
156 Akkermansia, and resulted in higher uveitis scores (Extended Data Fig. 4e-f). Akkermansia
157 was nearly undetectable in the PBS control group, whose gut microbiota became
158 dominated by Firmicutes (Extended Data Fig. 4g). As such, the relative abundances of
159 Akkermansia and Firmicutes showed a near-perfect inverse relationship (r-squared > 0.99,
160 $p < 0.0001$) (Extended Data Fig. 4h). Other bacterial phyla that are prominent in normal
161 mouse or human gut flora were low or on the borderline of detectability (Extended Data
162 Fig. 4i). Thus, this model reflects a minimal-diversity gut ecosystem dominated by the two
163 taxa that we hypothesize to display competitive dynamics that control expression of
164 disease.

165 Second paradigm: To examine this hypothesis under more physiological conditions, where
166 Akkermansia is not given a major “head start”, we associated GF R161H mice with flora
167 from HuFI mice (selected for low disease and low abundance of Akkermansia) “spiked”, or
168 not, with cultured *A. muciniphila* (Fig. 5a). Fecal microbiome profiling confirmed successful
169 microbial engraftment and stability of Akkermansia-high or Akk-low status (Fig. 5d &
170 Extended Data Fig. 5a). Akkermansia “spiked” flora induced more severe uveitis than base
171 HuFI alone (Fig. 5b-c) and the relative abundances of Akkermansia and Firmicutes were
172 consistently inversely correlated (Fig. 5e). Notably, among the major bacterial phyla,

173 Firmicutes was the only phylum whose abundance was decreased in Akk-enriched mice
174 (Fig. 5d & Extended Data Fig. 5b), particularly those taxa considered "professional" SCFA
175 producers[24] (Extended Data Fig. 5c). To confirm that the effects described above were
176 indeed Akkermansia-specific, we associated GF R161H mice with the same HuFl "spiked"
177 with *E. coli*. The disease-promoting phenotype and the reduction in Firmicutes abundance
178 were not recapitulated, supporting the notion that the observed effects were specific to
179 Akkermansia (Extended Data Fig. 5d-f). Together, these results reinforce a dynamic
180 balance between Akkermansia and Firmicutes that modulates autoimmune uveitis in a
181 physiologically relevant setting.

182 To mechanistically link Akkermansia–Firmicutes dynamics with circulating SCFA levels
183 available to regulate uveitis-relevant immune responses, we measured serum SCFAs and
184 host immune parameters. All three major SCFAs – acetic, butyric and propionic acids –
185 were reduced in Akk-high mice compared with Akk-low mice (Fig. 5f), consistent with the
186 negative relationship between Akkermansia and Firmicutes. This reduction was not
187 observed in the *E.coli* control group (Extended Data Fig. 5g). Given the known
188 immunomodulatory role of SCFAs[21] , we examined whether this metabolomic shift was
189 associated with an altered systemic effector response. In both the Akk-associated minimal
190 flora model and the Akk-enriched HuFl model, reduced serum SCFAs were tightly coupled
191 with elevated serum and/or gut IFN-γ responses (Fig. 5g–j). These results implicate that
192 SCFAs may regulate disease by dampening the Th1 effector response.

193 The final mechanistic question was whether Akkermansia can provide surrogate antigenic
194 stimuli to trigger activation of the R161H TCR-expressing cells in the gut[2]. To address this,
195 we used an *in vitro* activation assay, where naïve R161H CD4 T cells and antigen-
196 presenting cells were cultured with Akk-rich HuFl gut content extracts, or with heat-killed
197 Akkermansia. Unlike SPF gut flora extracts or the cognate peptide antigen[2,10], neither
198 Akkermansia preparation activated the retina-specific T cells, as measured by expression
199 of CD69 and Nur77 (Extended Data Fig. 6a-b), indicating that Akkermansia was not acting
200 as an antigen mimic.

201 Single cell RNA-seq analysis of colonic CD4 T cells, of which an average of 15%
202 expressed the R161H TCR, revealed that both R161H TCR-expressing and non-R161H
203 (endogenous) T cells had a Th1, rather than a Th17, signature, that positively correlated
204 with abundance of Akkermansia (Extended Data Fig. 6c). Akk-high colonic CD4 T cells
205 showed an increased proportion of Th1 cells with enriched interferon- and inflammation-
206 associated transcriptional programs (Stat1, Irf1, Cebpb, Jund), indicating an augmented
207 Th1 transcriptional profile (Extended Data Fig. 6d-e) and a broadly increased myeloid-to-
208 T cell signaling (Extended Data Fig. 6f), in which MHC class-II-associated APC–CD4
209 interactions favor Type 1 over Type 17 polarization (Extended Data Fig. 6g).

210 VDJ analysis did not reveal evidence for a 2nd TCR among R161H TCR+ cells, and *in*
211 *silico* analysis did not reveal shared sequence(s) between Akkermansia and IRBP$_{161-180}$,
212 which is the cognate R161H TCR epitope, supporting a mechanism independent of
213 cognate antigen recognition. Together, these findings support a model in which
214 Akkermansia regulates disease and shapes the T-cell effector response at 2 levels:
215 directly, through innate, adjuvant-like mechanisms modulating APC-T cell interactions, as
216 well as indirectly, by modulating SCFA-producing Firmicutes. This working model is
217 depicted in Figure 6a.

218 **6. The inverse relationship between Verrucomicrobia and Firmicutes extends to**
219 **clinical uveitis, multiple sclerosis and Crohn's disease**

220 Because effector Th1 skewing in the Akk-rich gut environment was independent of
221 antigenic specificity, we hypothesized that it could be associated with human
222 inflammatory conditions, such as uveitis, multiple sclerosis (MS) and inflammatory bowel
223 disease (IBD). To establish a common metric for comparing healthy to diseased state, we
224 used the phylum-level ratio of Verrucomicrobia / Firmicutes (V/F ratio) which consistently
225 tracked with disease severity in HuFI mice (Fig. 6b-c). Application of this metric to the
226 entire cohort of our clinical uveitis samples (so as to minimize any selection bias),
227 revealed higher V/F ratios in uveitis patients compared to healthy subjects (Fig. 6d). We
228 next examined publicly available MS[25] and IBD[26] datasets, the latter comprising patients
229 with Crohn's disease and ulcerative colitis (UC). Compared to healthy controls, the V/F

230 ratio in MS, and in Crohn's disease patients—a condition predominantly driven by Th1-
231 mediated inflammation—but not in UC patients[27,28], was markedly elevated (Fig. 6e-f).
232 Taken together, the gut microbial interaction networks indicated a negative correlation of
233 Verrucomicrobia (Akkermansia) with Firmicutes not only in R161H mice, but also in
234 uveitis, MS and Crohn's disease patients, supporting the generality of this relationship.

235

236 **DISCUSSION**

237 In this study, we report a gut microbial interaction network that regulates autoimmune and
238 inflammatory processes along the "gut–eye axis". By integrating data-driven analyses
239 and *in vivo* microbial perturbation, we provide compelling evidence for a negative
240 relationship between Akkermansia and Firmicutes and link it to disease severity.
241 Specifically, Akkermansia appears to promote sEAU in HuFl R161H mice by
242 outcompeting SCFA-producing Firmicutes in the gut, resulting in diminished SCFA levels
243 and enhanced Th1 responses both locally and systemically (Fig. 6a). Our findings
244 provide a mechanistic basis for how the gut microbiome impacts ocular autoimmunity,
245 dissect the complex interacting stimuli that underpin this process, and highlight its broadly
246 generalizable nature.

247 Our network-based perspective contrasts with previous studies, which have mostly
248 focused on how individual gut microbial taxa influence disease and host immunity[4].
249 *A. muciniphila* has been implicated across a spectrum of inflammatory and autoimmune
250 diseases[29]. However, different reports have described conflicting functional effects. As an
251 example, Akkermansia has been reported to promote Th1 polarization of human
252 PBMCs[30], and its relative abundance correlated with disease activity in MS patients[25,30-
253 32]. In contrast, in vivo Th1-polarizing activity has not been observed in Akk-
254 monocolonized mice[30] and T cell responses to Akkermansia in SPF mice have not
255 correlated with a consistent T cell effector phenotype[33]. These observations, together
256 with our finding that Akkermansia affects sEAU through interactions that modulate the
257 broader microbial network, support the notion that the immunological impact of

258 Akkermansia—and of any single microbes in general—depends heavily on microbial
259 community context and host factors.

260 The R161H sEAU model provides a platform to dissect these contextual effects. When
261 the model was first established, we identified signaling by a (microbiota-dependent)
262 mimic antigen in the SPF flora of R161H mice as an important, but possibly not the only,
263 disease trigger[2]. In the case of Akkermansia as a disease-promoting influence that does
264 not appear to act as a surrogate antigen, it is likely that other HuFI member(s) may
265 provide this function. The preferential enhancement of MHC-II–associated APC–CD4
266 interactions in Akkermansia-enriched gut is conceptually reminiscent of the SFB-driven
267 Th17 program[34,35], in which dendritic-cell MHC-II presentation and commensal-specific
268 TCR selection create a Th17-polarizing milieu that instructs adaptive effector
269 differentiation. Akk seems to promote a polarizing milieu encouraging Th1 programming
270 of CD4+ cells without evidence for IRBP-specific microbial antigen mimicry.

271 We did not attempt to identify the HuFI microbial mimic, as identifying it would lack
272 translational relevance. The R161 TCR recognizes a mouse class II (I-A^r)-restricted
273 epitope of IRBP. Human MHC class II molecules would almost certainly present a
274 different epitope(s) from any given antigen than does mouse I-A^r, plus the epitope(s)
275 would differ between individuals, given the heterogeneity of human MHC haplotypes.
276 Moreover, whereas IRBP is a dominant retinal autoantigen in mice, human uveitis more
277 commonly involves recall responses to arrestin[1]. Therefore, although the HuFI R161H
278 sEAU model cannot reveal specific antigenic targets involved in human uveitis, it can
279 reveal conserved mechanisms shared across species, such as the microbial interaction
280 network identified in this study.

281 A key feature of this microbial network is the negative relationship between Akkermansia
282 and Firmicutes, which links gut microbial composition to systemic inflammation. This
283 antagonism likely arises from multiple, non-mutually exclusive mechanisms. Both taxa
284 are dominant colonizers of the colon and may engage in direct niche competition and
285 indirect interactions. Akkermansia promotes mucus degradation during gut
286 inflammation[36,37]. The compromised mucus barrier would exacerbate inflammation and

287 oxidative stress[38], creating inhospitable conditions for obligate anaerobes like Firmicutes.
288 Finally, while Akk antagonizes SCFA-producing Firmicutes, their SCFAs can in turn act to
289 suppress Akkermansia growth and mucolytic activity[39].

290 All those interactions are reflected in the V/F ratio, which may serve as an indicator of
291 inflammatory state and immune polarization across species, supporting its translational
292 value. A similar "legacy" metric Firmicutes to Bacteroidetes (F/B ratio) has been used to
293 indicate overall shifts in gut microbiome composition, but is now being phased out due to
294 its inconsistent disease associations[40,41]. We propose that the V/F ratio is more
295 specifically informative in autoimmune and inflammatory settings.

296 Of note, numerous studies report an association between uveitic diseases and gut
297 inflammation. Uveitis is associated with an increased risk of Crohn's (but not of UC)[42],
298 and Crohn's patients are more likely than UC patients to develop uveitis[43]. The findings
299 are compatible with the notion that the V/F ratio increases under conditions where gut
300 inflammation co-occurs with extraintestinal autoimmunity. The V/F ratio may also rise
301 under Th1-dominant inflammatory conditions, as observed in our data. Our analyses
302 reveal elevated V/F ratios not only in our patients with uveitis, but also in published
303 datasets from patients with MS[25] and IBD[26]. Within IBD, increases in V/F were evident in
304 Crohn's disease (Th1-dominant[44-46]), but not in UC (Th2-like[47-49]).

305 Limitations of the study: The complexity of the Akkermansia–Firmicutes axis poses a
306 major challenge to resolving microbial relationships at species and strain levels.
307 Emerging approaches such as bacterial spatial transcriptomics[50] are not yet sufficiently
308 developed to dissect mechanisms by which Akkermansia antagonizes SCFA-
309 producing Firmicutes. That said, outcompetition could involve physical elimination via
310 bacteriocins acting on SCFA producers[51]. In addition, the asynchronous nature of
311 disease development in individual mice and the limited capacity of our GF R161H colony
312 constrains the scale and breadth of experiments. Consequently, some types of
313 mechanistic studies, including administering individual SCFAs to HuFI mice for functional
314 validation, could not be accommodated.

315 In conclusion, our findings show that a complex microbial interaction network—rather
316 than individual taxa—plays a central role in shaping the gut–eye axis. The Akkermansia–
317 Firmicutes relationship likely represents a generalizable ecological principle in which
318 microbial competition influences systemic immune balance and susceptibility to

319 autoimmunity and inflammation, and which extends across species. Future studies aimed
320 at defining the mechanisms by which Akkermansia gains an advantage over SCFA-
321 producing Firmicutes, may guide the development of microbiome-based interventions for
322 autoimmune and inflammatory diseases that intersect with gut dysregulation.
323
324
325 **METHODS**

326 ***Mice.*** R161H mice on the B10.RIII background[10] were bred in-house and maintained
327 under SPF conditions and fed standard facility chow *ad libitum*. GF and HuFI R161H
328 mice were maintained in the gnotobiotic isolators. The animal study protocol (NEI-688)
329 was approved by the NEI Institutional Animal Care and Use Committee.

330 ***Generation of gnotobiotic mice with human stool samples.*** Human stool samples of
331 healthy volunteers were collected at Keio University according to the study protocol[52]
332 approved by the Institutional Review Boards (approval number 20150075) and informed
333 consent was obtained from each subject. Stool samples were suspended in 20% glycerol
334 in PBS, snap frozen in liquid nitrogen and stored at -80°C. The U, V, and W stocks were
335 thawed and gavaged into GF R161H mice and individual cohort lines were established in
336 separate gnotobiotic isolators.

337 ***Evaluation of uveitis phenotype.*** Development of uveitis was monitored by fundoscopic
338 observation via a binocular microscope of anesthetized mice at the indicated age. For
339 histopathology, eyes were enucleated and fixed in 4% glutaraldehyde for 1 h and
340 transferred to 10% formaldehyde for additional 24 h, embedded in methacrylate, and
341 processed for H&E staining. Disease scores of fundoscopy and histology were assigned
342 by a masked observer on a scale of 0–4, according to the criteria for EAU scoring
343 described in detail elsewhere which are based on the number, size and type of lesions[53].

344 ***HuFI R161H fecal suspension preparation.*** Cecal and colonic contents from HuFI mice
345 of varying disease severity were collected under sterile conditions and immediately
346 transferred on ice to an anaerobic chamber (Coy Laboratory Products). Contents were
347 filtered three times through a 70 μm cell strainer in 20% glycerol–PBS, and aliquoted to

348 prevent repeated freeze–thaw cycles. Each sample was prepared from either individual
349 mice or pools of mice with the same disease severity. The baseline HuFl suspension for
350 reconstitution experiments was prepared from two mice with low uveitis scores and
351 validated by 16S sequencing to contain ~1% Akkermansia (ranges 1–8% in tested
352 samples).

353 ***In vivo microbial enrichment by gnotobiotic reconstitution.*** *A. muciniphila* or *E. coli*
354 were cultured in mucin-BHI media inside the anaerobic chamber or in LB media in the
355 aerobic incubator, respectively. Microbial monoculture was prepared in advance and the
356 first passage timed to reach the exponential growth phase immediately prior to oral
357 gavage. On the day of gavage, GF R161H were transferred from the gnotobiotic isolators
358 to sterile and static microisolator cages with a Reemay filter top. Using sterile techniques,
359 these mice were examined by fundoscopy and assigned to experimental or control
360 groups based on initial uveitis disease scores (<1), age (4-7 weeks) and sex. While mice
361 were recovering from anesthesia, gavage material was prepared inside the anaerobic
362 chamber for *A. muciniphila* or in the aerobic bacterial hood for *E. coli*, or sterile PBS,
363 which in the "HuFl base model" was combined with the selected HuFl fecal suspension,
364 so each mouse in the experimental group would receive an additional ~10^8 CFU of the
365 microbe of interest in 200uL HuFl fecal suspension via oral gavage. Fecal sampling and
366 fundoscopy scoring were performed on a weekly basis, and mice were handled under
367 sterile protocols, with cages opened only inside a biosafety cabinet.

368 ***Fecal DNA extraction and quantification of microbes.*** Fecal pellets were collected
369 from individual mice, immediately frozen on dry ice and stored at -80°C until bacterial
370 DNA extraction in house as previously described[54] or by the NCI Genetics and
371 Microbiome Core. Absolute abundance of bacteria in each fecal sample was assessed by
372 quantitative polymerase chain reaction (qPCR) using Akkermansia or *E. coli* standard
373 curves with Fast SYBR Green Supermix (Applied Biosystems, Waltham, MA, USA) and
374 run on a QuantStudio™ 7 Pro Real-Time PCR System (Applied Biosystems). Specific
375 primers for Akkermansia were Akk.mu3.Fwd (5'- GCGTAGGCTGTTTCGTAAGTCGTGT
376 GTGAAAG -3') and Akk.mu3.Rvs (5'-GAGTGTTCCCGATATCTACGCATTTCA -3')[55],
377 and for *E. coli* were Uni515F (5'- GTGCCAGCMGCCGCGGTAA -3') and Ent826R (5'-

378 GCCTCAAGGGCACAACCTCCAAG -3')[56]. Five ng of fecal DNA was amplified per 10 µL
379 reaction with the following cycling conditions: initial denaturation at 95 °C for 20 sec,
380 followed by 40 cycles of 95 °C for 3 sec and 63 °C for 30 sec. A melt-curve analysis was
381 included at the end of each run to confirm amplification specificity. Bacterial counts (CFU)
382 per 5 ng of DNA were extrapolated from fitted standard curves correlating Cq values with
383 bacterial quantity.

384 ***16S rRNA gene sequencing and analyses.*** Fecal samples were processed at the NCI
385 Genetics and Microbiome Core for 16S rRNA gene sequencing as detailed in prior
386 work[54]. 16S amplicon sequence variants (ASV) were inferred with YAMS16 v1.7
387 (https://github.com/jhbadger/YAMS16), a pipeline running DADA2[57], and taxonomically
388 classified using the SILVA reference database (release 138.1)[58]. Microbial diversity,
389 differential abundance and multivariable association analyses were performed with
390 phyloseq v1.42.0[59], MaAsLin2 v1.12.0[60], microViz v0.12.3[61] in R. Microbial association
391 networks were analyzed with NetCoMi[62].

392 ***Shotgun metagenomic sequencing and analyses.*** Selected DNA samples were
393 submitted to CosmosID, Inc. (Germantown, MD, USA) for shallow shotgun sequencing (3
394 million reads per sample). Specifically, DNA libraries were prepared using the Nextera XT
395 DNA Library Preparation Kit (Illumina, Inc., San Diego, CA, USA) and IDT Unique Dual
396 Indexes with total DNA input of 1 ng. Genomic DNA was fragmented using a proportional
397 amount of Illumina Nextera XT fragmentation enzyme. Unique dual indexes were added
398 to each sample followed by 12 cycles of PCR to construct libraries. DNA libraries were
399 purified using AMpure magnetic Beads (Beckman Coulter, Inc., Brea, CA, USA) and
400 eluted in QIAGEN EB buffer. DNA libraries were quantified using Qubit 4 fluorometer and
401 Qubit™ dsDNA HS Assay Kit. Libraries were then sequenced on the Element AVITI
402 platform 2x150 bp. JAMS v1.9.9[63] and HUMAnN v3.9[64] were used for taxonomic and
403 functional profiling, and genes involved in metabolic pathways of the main SCFAs
404 (acetate, butyrate and propionate) were identified based on InterPro, Gene Ontology and
405 Pfam annotations, and those present in the uveitis datasets were compared between
406 diseased and healthy groups.

407 ***Targeted metabolomics and cytokine quantification.*** Cecal and colonic contents
408 (collectively referred to as "fecal contents"), eyes, and serum were collected from age-
409 matched mice at harvest. Eyes were fixed for histological analysis as described above.
410 Fecal and serum samples were snap-frozen on dry ice and stored at −80 °C. For
411 metabolite profiling, at least 100 mg of fecal contents and 150 µL of serum per mouse
412 were transferred to designated tubes and shipped on dry ice to Metabolon, Inc.
413 (Morrisville, NC, USA) for absolute quantification of eight short-chain fatty acids (acetic,
414 propionic, butyric, isobutyric, 2-methylbutyric, valeric, isovaleric, and hexanoic acids).
415 Serum cytokine concentrations were measured using the Mouse Inflammation Panel (13-
416 plex, LEGENDplex™, BioLegend, San Diego, CA, USA) according to the manufacturer's
417 instructions. Data were acquired on a CytoFlex LX flow cytometer (Beckman coulter) and
418 analyzed with LEGENDplex Data Analysis Software (BioLegend) to quantify cytokine
419 levels based on standard curves.

420 ***Tissue harvesting and flow cytometry analyses.*** Peripheral lymphoid tissues
421 (submandibular lymph nodes, spleen, peripheral lymph nodes, mesenteric lymph nodes),
422 and gut lamina propria from small intestine and colon were collected and prepared for
423 single cell suspensions as described elsewhere[2]. Cells were stained at the dilution of
424 1:1000 with fluorochrome-conjugated antibodies (clones) from BD Biosciences,
425 BioLegend or eBioscience/Thermo Fisher Scientific. Surface staining panel: FITC-TCR
426 beta chain (H57-597), BB700-CD69 (H1.2F3), PE-CD62L (MEL-14), PE/Dazzle594
427 CD183/CXCR3 (CXCR3-173), PE/Cy7-CD199/CCR9 (CW-1.2), Alexa Fluor 700 CD8a
428 (53-6.7), APC-eFluor 780-CD44 (IM7), Brilliant Violet (BV) 421-CD103 (2E7), BV510-
429 CD45 (30-F11), BV650-CD4 (RM4-5), BV785-CD196/CCR6 (29-2L17), BUV496-CD3
430 (145-2C11). Intracellular staining panel: Alexa Fluor 488-IL-17F (9D3.1C8),
431 PerCP/Cyanine5.5-T-bet (4B10), PE-RORgt (Q31-378) PE/Dazzle594-IL-10 (JES5-
432 16E3), PE/Cy7-GM-CSF (MP1-22E9), APC-IL-22 (IL22JOP), Alexa Fluor 700-Foxp3
433 (FJK-16s), APC-eFluor 780-CD8a (53-6.7), BV421-IFN-g (XMG1.2), BV510-CD4 (RM4-
434 5), BV650-IL-17A (TC11-18H10), BV786-CD44 (IM7), BUV496-CD3 (145-2C11). Dead
435 cells were excluded by staining with ViaKrome 808 Fixable Viability Dye from Beckman
436 Coulter. Fluorescence-activated cell sorting analyses were done using CytoFlex LX
437 (Beckman coulter). FlowJo v10 (BD Biosciences) was used for data analyses.

438 ***In vitro activation assay on retina-specific T cells.*** IRBP-specific T cells were
439 harvested from spleen and peripheral lymph nodes of *Tcra*$^{-/-}$ *Nr4a1*^{EGFP} (Nur77^{GFP})
440 R161H mice and were enriched for naïve CD4^{+} cells by negative selection using Mouse
441 Streptavidin Rapidsphere Isolation Kit (EasySep, StemCell Technologies). The following
442 biotin-conjugated anti-mouse antibodies (clones) from BioLegend, BD Biosciences were
443 used at 1:250 dilutions: CD8 (53-6.7), CD11b (M1/70), CD11c (N418), CD16/32 (93),
444 CD19 (6D5), CD24 (M1/69), CD25 (PC61), CD49b (DX5) CD69 (H1.2F3), CD45R/B220
445 (RA3-6B2), Ly-6G/Ly-6C (Gr1, RB-8C5), I-A/I-E (M5/114.15.2), NK1.1 (PK136), $\gamma\delta$TCR
446 (GL3), Ter 119 (TER-119). CD11c^{+} dendritic cells were purified from spleen of WT
447 B10.RIII mice as antigen-presenting cells using CD11c MicroBeads Ultrapure (Miltenyi
448 Biotec). T cells and dendritic cells were co-cultured at a 4:1 ratio in the presence of heat-
449 killed *A. muciniphila* (95°C for 5 min), heat-killed *E. coli* (60°C for 30 min), or bacteria-rich
450 extracts from the gut content[2]. T cell activation was assessed after 22 h by flow
451 cytometric analysis of CD69 and Nur77 expression.

452 ***5' single cell RNAseq sample processing.*** Cells from colon LP were labeled with
453 TotalSeq C anti-mouse HashTags 1-10 (C0301-C0310, clones M1/42; 30-F11) and 14
454 cell surface antibodies from BioLegend at the dilution of 1:100. Cell surface anti-mouse
455 antibodies: CD4 (DNA_ID C0001, clone RM4-5), CD8a (C0002, 53-6.7), Ly-6C (C0013,
456 HK1.4), CD11b (C0014, M1/70), Ly-6G (C0015, 1A8), CD90.2 (C0075, 30-H12), CD19
457 (C0093, 6D5), CD11c (C0106, N418), F4/80 (C0114, BM8), I-A/I-E (C0117,
458 M5/114.15.2), NK-1.1 (C0118, PK136), TCRβ chain (C0120, H57-597), TCR g/d (C0121,
459 GL3), and CD3 (C0182, 17A2). Labeled cells were sorted for live CD45^{+} and CD4^{+}
460 populations with PE anti-mouse CD45.2 (clone 104, BioLegend), eFluor™ 450 anti-
461 mouse CD4 (clone RM4-5, eBioscience) and 7-AAD (eBioscience) using
462 FACSAria III/Fusion sorters (BD Biosciences). Post-sort viability exceeded 80%, and
463 hash-tagged samples were pooled at equal ratios within each experimental group,
464 combining CD45^{+} and CD4^{+} fractions at 1:1 ratio to enrich for CD4^{+} T cells. Pooled cells
465 were resuspended in PBS with 0.04% BSA and loaded onto a 10x Genomics Chromium
466 X instrument at 700–1200 cells/μL for single cell 5' gene expression and TCR profiling.
467 Libraries were prepared using the Chromium Next GEM Single Cell 5' Reagent Kits v2

468 (Dual Index) following the manufacturer's protocol, and sequenced on NovaSeq 6000
469 platform (Illumina, Inc., San Diego, CA, USA).

470 ***Single cell RNAseq data analyses.*** Six mice (three from each group) were used for
471 analyses. Sequencing data were processed with Cell Ranger v9.0.1 (10x Genomics) for
472 demultiplexing and alignment to the Mus musculus reference (GRCm39, Genome
473 Reference Consortium, 2024). Cell doublets were detected and removed using Scrublet
474 v0.2.3[65]. Cells exhibiting high mitochondrial transcript content (≥ 5%) or abnormal gene
475 counts (< 500 or > 8000) were excluded. Expression data were log-normalized and
476 scaled using the Scanpy v1.11.0[66] in Python v3.10. Dimensionality reduction was
477 performed using Principal Component Analysis (PCA) followed by Uniform Manifold
478 Approximation and Projection (UMAP), and cell clusters were identified with the Leiden
479 algorithm[67]. Cell type annotation was based on computational classification using SingleR
480 v2.8.0[68] with mouse immune reference data from celldex::ImmGenData v1.16.0 in R v4.4,
481 as well as the expression of canonical cell type marker genes, and validated by cell
482 lineage–specific surface antibody. The expression of both Trav16 and Trbv5 in a CD4 T
483 cell was the standard used to identify IRBP-specific T cells[10]. Seurat v5.1.0[69] was also
484 used to generate object files for downstream application of CellChat[70] and SCENIC[71] in
485 the R environment. CellChat was applied to infer changes in the strongest cell-cell
486 interactions between Th1 cells and other cell types in the colon LP in Akk-rich mouse.
487 SCENIC was used to reconstruct gene regulatory networks and to assess transcription
488 factor activity at the single-cell level, enabling identification of Akkermansia-associated
489 alterations in Th1 cell programming and lineage maintenance.

490 ***NEI clinical samples and public human data.*** Stool samples were obtained from
491 patients with autoimmune uveitis and healthy controls enrolled in a clinical cohort at the
492 NEI, NIH. All participants provided written informed consent under the protocol approved
493 by the Institutional Review Board (Protocol 13-EI-0072). A stratified cohort of treatment-
494 naïve autoimmune uveitis was selected for in-depth gut microbial network analysis,
495 representing primarily posterior- and pan-uveitis cases and ocular-restricted phenotypes
496 such as idiopathic uveitis and birdshot chorioretinopathy. 16S rRNA gene and shotgun
497 metagenomic sequencing of human fecal samples were performed by the Microbiome

498 Cores at the NCI and the Goodman-Luskin Microbiome Center (Los Angeles, CA, USA).
499 Public microbiome data of IBD patients' stool are from PRJNA1198911[26], and that of MS
500 patient stool from the International MS Microbiome Study (iMSMS)[25].

501 ***Statistical analyses.*** Statistical analyses were conducted with R v4.4, Python v3.10, and
502 GraphPad Prism v10.5.0. Non-parametric tests such as Mann-Whitney U and Kruskal-
503 Wallis tests were used for most comparisons between two or more groups. Group
504 differences in multivariate community structure were evaluated by Permutational
505 Multivariate Analysis of Variance (PERMANOVA). Pearson's or Spearman's rank
506 correlation, as well as multivariable association (MaAsLin2 and equivalent methods) were
507 used to assess associations between microbial features and disease or immune
508 phenotypes. P-values were adjusted for multiple comparisons using the false discovery
509 rate (FDR) where applicable, and statistical significance was indicated as follows: * $P <$
510 0.05, ** $P < 0.01$, *** $P < 0.001$, and **** $P < 0.0001$. Data in bar plots are presented as
511 mean values ± SEMs.

512 ***Data availability.*** Raw microbiome sequencing data, including 16S rRNA gene amplicon
513 and shotgun metagenomic sequencing reads from mouse samples and de-identified
514 human samples, have been deposited in the NCBI Sequence Read Archive (SRA) under
515 BioProject ID PRJNA1451962. Raw and processed single-cell RNA sequencing data
516 have been deposited in the Gene Expression Omnibus (GEO) under accession number
517 GSE327793.

518 ***Code availability.*** No custom code was developed for this study. All analyses were
519 performed using publicly available software packages, and the specific versions and
520 parameters used are described in the Methods section.

521

522

523 **REFERENCES**

524 1 Caspi, R. R. A look at autoimmunity and inflammation in the eye. *J Clin Invest* **120**, 3073-
525 3083 (2010).

526 2 Horai, R. *et al.* Microbiota-Dependent Activation of an Autoreactive T Cell Receptor
527 Provokes Autoimmunity in an Immunologically Privileged Site. *Immunity* **43**, 343-353
528 (2015).

529 3 Horai, R. & Caspi, R. R. Microbiome and Autoimmune Uveitis. *Front Immunol* **10**, 232
530 (2019).

531 4 Salvador, R., Zhang, A., Horai, R. & Caspi, R. R. Microbiota as Drivers and as Therapeutic
532 Targets in Ocular and Tissue Specific Autoimmunity. *Front Cell Dev Biol* **8**, 606751 (2020).

533 5 White, Z. *et al.* Gut inflammation promotes microbiota-specific CD4 T cell-mediated
534 neuroinflammation. *Nature* **643**, 509-518 (2025).

535 6 Lee, H. G. *et al.* Pathogenic function of bystander-activated memory-like CD4(+) T cells in
536 autoimmune encephalomyelitis. *Nat Commun* **10**, 709 (2019).

537 7 Miller, S. D. *et al.* Persistent infection with Theiler's virus leads to CNS autoimmunity via
538 epitope spreading. *Nat Med* **3**, 1133-1136 (1997).

539 8 Deeg, C. A., Amann, B., Raith, A. J. & Kaspers, B. Inter- and intramolecular epitope spreading
540 in equine recurrent uveitis. *Invest Ophthalmol Vis Sci* **47**, 652-656 (2006).

541 9 Ji, Q., Perchellet, A. & Goverman, J. M. Viral infection triggers central nervous system
542 autoimmunity via activation of CD8+ T cells expressing dual TCRs. *Nat Immunol* **11**, 628-634
543 (2010).

544 10 Horai, R. *et al.* Breakdown of immune privilege and spontaneous autoimmunity in mice
545 expressing a transgenic T cell receptor specific for a retinal autoantigen. *J Autoimmun* **44**,
546 21-33 (2013).

547 11 Nakamura, Y. K. *et al.* Gut Microbial Alterations Associated With Protection From
548 Autoimmune Uveitis. *Invest Ophthalmol Vis Sci* **57**, 3747-3758 (2016).

549 12 Shimizu, J. *et al.* Bifidobacteria Abundance-Featured Gut Microbiota Compositional Change
550 in Patients with Behcet's Disease. *PLoS One* **11**, e0153746 (2016).

551 13 Huang, X. *et al.* Gut Microbiota Composition and Fecal Metabolic Phenotype in Patients
552 With Acute Anterior Uveitis. *Invest Ophthalmol Vis Sci* **59**, 1523-1531 (2018).

553 14 Kalyana Chakravarthy, S. *et al.* Dysbiosis in the Gut Bacterial Microbiome of Patients with
554 Uveitis, an Inflammatory Disease of the Eye. *Indian J Microbiol* **58**, 457-469 (2018).

555 15 Ye, Z. *et al.* A metagenomic study of the gut microbiome in Behcet's disease. *Microbiome* **6**,
556 135 (2018).

557 16 Ye, Z. *et al.* Altered gut microbiome composition in patients with Vogt-Koyanagi-Harada
558 disease. *Gut Microbes* **11**, 539-555 (2020).

559 17 Steimle, A. *et al.* Gut microbial factors predict disease severity in a mouse model of multiple
560 sclerosis. *Nat Microbiol* **9**, 2244-2261 (2024).

561 18 Luger, D. *et al.* Either a Th17 or a Th1 effector response can drive autoimmunity: conditions
562 of disease induction affect dominant effector category. *J Exp Med* **205**, 799-810 (2008).

563 19 Damsker, J. M., Hansen, A. M. & Caspi, R. R. Th1 and Th17 cells: adversaries and
564 collaborators. *Ann N Y Acad Sci* **1183**, 211-221 (2010).

565 20 Horai, R. & Caspi, R. R. Cytokines in autoimmune uveitis. *J Interferon Cytokine Res* **31**, 733-
566 744 (2011).

567 21 Mann, E. R., Lam, Y. K. & Uhlig, H. H. Short-chain fatty acids: linking diet, the microbiome
568 and immunity. *Nat Rev Immunol* **24**, 577-595 (2024).

569 22 Nakamura, Y. K. *et al.* Short chain fatty acids ameliorate immune-mediated uveitis partially
570 by altering migration of lymphocytes from the intestine. *Sci Rep* **7**, 11745 (2017).

571 23 Chen, X. *et al.* Sodium butyrate regulates Th17/Treg cell balance to ameliorate uveitis via
572 the Nrf2/HO-1 pathway. *Biochem Pharmacol* **142**, 111-119 (2017).

573 24 Louis, P. & Flint, H. J. Formation of propionate and butyrate by the human colonic
574 microbiota. *Environ Microbiol* **19**, 29-41 (2017).

575 25 iMSMS Consortium. Gut microbiome of multiple sclerosis patients and paired household
576 healthy controls reveal associations with disease risk and course. *Cell* **185**, 3467-3486 e3416
577 (2022).

578 26 Orejudo, M. *et al.* Exploration of fecal microbiota in newly diagnosed patients with
579 inflammatory bowel disease using shotgun metagenomics. *Front Cell Infect Microbiol* **15**,
580 1595884 (2025).

581 27 Strober, W., Fuss, I. & Mannon, P. The fundamental basis of inflammatory bowel disease. *J*
582 *Clin Invest* **117**, 514-521 (2007).

583 28 Guan, Q. A Comprehensive Review and Update on the Pathogenesis of Inflammatory Bowel
584 Disease. *J Immunol Res* **2019**, 7247238 (2019).

585 29 Cani, P. D., Depommier, C., Derrien, M., Everard, A. & de Vos, W. M. Akkermansia
586 muciniphila: paradigm for next-generation beneficial microorganisms. *Nat Rev*
587 *Gastroenterol Hepatol* **19**, 625-637 (2022).

588 30 Cekanaviciute, E. *et al.* Gut bacteria from multiple sclerosis patients modulate human T cells
589 and exacerbate symptoms in mouse models. *Proc Natl Acad Sci U S A* **114**, 10713-10718
590 (2017).

591 31 Berer, K. *et al.* Gut microbiota from multiple sclerosis patients enables spontaneous
592 autoimmune encephalomyelitis in mice. *Proc Natl Acad Sci U S A* **114**, 10719-10724 (2017).

593 32 Jangi, S. *et al.* Alterations of the human gut microbiome in multiple sclerosis. *Nat Commun*
594 **7**, 12015 (2016).

595 33 Ansaldo, E. *et al.* Akkermansia muciniphila induces intestinal adaptive immune responses
596 during homeostasis. *Science* **364**, 1179-1184 (2019).

597 34 Goto, Y. *et al.* Segmented filamentous bacteria antigens presented by intestinal dendritic
598 cells drive mucosal Th17 cell differentiation. *Immunity* **40**, 594-607 (2014).

599 35 Yang, Y. *et al.* Focused specificity of intestinal TH17 cells towards commensal bacterial
600 antigens. *Nature* **510**, 152-156 (2014).

601 36 Desai, M. S. *et al.* A Dietary Fiber-Deprived Gut Microbiota Degrades the Colonic Mucus
602 Barrier and Enhances Pathogen Susceptibility. *Cell* **167**, 1339-1353 e1321 (2016).

603 37 Tingler, A. M. & Engevik, M. A. Breaking down barriers: is intestinal mucus degradation by
604 Akkermansia muciniphila beneficial or harmful? *Infect Immun* **93**, e0050324 (2025).

605 38 Sugihara, K. *et al.* Mucolytic bacteria license pathobionts to acquire host-derived nutrients
606 during dietary nutrient restriction. *Cell Rep* **40**, 111093 (2022).

607 39 Schwabkey, Z. I. *et al.* Diet-derived metabolites and mucus link the gut microbiome to fever
608 after cytotoxic cancer treatment. *Sci Transl Med* **14**, eabo3445 (2022).

609 40 Magne, F. *et al.* The Firmicutes/Bacteroidetes Ratio: A Relevant Marker of Gut Dysbiosis in
610 Obese Patients? *Nutrients* **12** (2020).

611 41 Walters, W. A., Xu, Z. & Knight, R. Meta-analyses of human gut microbes associated with
612 obesity and IBD. *FEBS Lett* **588**, 4223-4233 (2014).

613 42 Lo, T. C., Chen, Y. Y. & Chen, H. H. Risk of inflammatory bowel disease in uveitis patients: a
614 population-based cohort study. *Eye (Lond)* **36**, 1288-1293 (2022).

615 43 Lin, H. *et al.* Differences in the prevalence of uveitis between Crohn's disease and ulcerative
616 colitis: A systematic review and meta-analysis. *Acta Ophthalmol* **102**, e485-e492 (2024).

617 44 Bouma, G. & Strober, W. The immunological and genetic basis of inflammatory bowel
618 disease. *Nat Rev Immunol* **3**, 521-533 (2003).

619 45 Fuss, I. J. *et al.* Disparate CD4+ lamina propria (LP) lymphokine secretion profiles in
620 inflammatory bowel disease. Crohn's disease LP cells manifest increased secretion of IFN-

621 gamma, whereas ulcerative colitis LP cells manifest increased secretion of IL-5. *J Immunol*
622 **157**, 1261-1270 (1996).

623 46 Parronchi, P. *et al.* Type 1 T-helper cell predominance and interleukin-12 expression in the
624 gut of patients with Crohn's disease. *Am J Pathol* **150**, 823-832 (1997).

625 47 Fuss, I. J. *et al.* Nonclassical CD1d-restricted NK T cells that produce IL-13 characterize an
626 atypical Th2 response in ulcerative colitis. *J Clin Invest* **113**, 1490-1497 (2004).

627 48 Heller, F. *et al.* Interleukin-13 is the key effector Th2 cytokine in ulcerative colitis that
628 affects epithelial tight junctions, apoptosis, and cell restitution. *Gastroenterology* **129**, 550-
629 564 (2005).

630 49 Strober, W. & Fuss, I. J. Proinflammatory cytokines in the pathogenesis of inflammatory
631 bowel diseases. *Gastroenterology* **140**, 1756-1767 (2011).

632 50 Sarfatis, A., Wang, Y., Twumasi-Ankrah, N. & Moffitt, J. R. Highly multiplexed spatial
633 transcriptomics in bacteria. *Science* **387**, eadr0932 (2025).

634 51 Montgomery, T. L. *et al.* Lactobacillaceae differentially impact butyrate-producing gut
635 microbiota to drive CNS autoimmunity. *Gut Microbes* **16**, 2418415 (2024).

636 52 Tanoue, T. *et al.* A defined commensal consortium elicits CD8 T cells and anti-cancer
637 immunity. *Nature* **565**, 600-605 (2019).

638 53 Horai, R. & Caspi, R. R. in *Animal Models for Retinal Diseases. Neuromethods.* Vol. 46 207-
639 225 (SpringerLink, 2010).

640 54 Salvador, R. *et al.* Too Much of a Good Thing: Extended Duration of Gut Microbiota
641 Depletion Reverses Protection From Experimental Autoimmune Uveitis. *Invest Ophthalmol*
642 *Vis Sci* **64**, 43 (2023).

643 55 Goux, H. J., Chavan, D., Crum, M., Kourentzi, K. & Willson, R. C. Akkermansia muciniphila as
644 a Model Case for the Development of an Improved Quantitative RPA Microbiome Assay.
645 *Front Cell Infect Microbiol* **8**, 237 (2018).

646 56 Barman, M. *et al.* Enteric salmonellosis disrupts the microbial ecology of the murine
647 gastrointestinal tract. *Infect Immun* **76**, 907-915 (2008).

648 57 Callahan, B. J. *et al.* DADA2: High-resolution sample inference from Illumina amplicon data.
649 *Nat Methods* **13**, 581-583 (2016).

650 58 Quast, C. *et al.* The SILVA ribosomal RNA gene database project: improved data processing
651 and web-based tools. *Nucleic Acids Res* **41**, D590-596 (2013).

652 59 McMurdie, P. J. & Holmes, S. phyloseq: an R package for reproducible interactive analysis
653 and graphics of microbiome census data. *PLoS One* **8**, e61217 (2013).

654 60 Mallick, H. *et al.* Multivariable association discovery in population-scale meta-omics studies.
655 *PLoS Comput Biol* **17**, e1009442 (2021).

656 61 Barnett, D. J. M., Arts, I. C. W. & Penders, J. microViz: an R package for microbiome data
657 visualization and statistics. *J Open Source Software* **6** 3201 (2021).

658 62 Peschel, S., Muller, C. L., von Mutius, E., Boulesteix, A. L. & Depner, M. NetCoMi: network
659 construction and comparison for microbiome data in R. *Brief Bioinform* **22** (2021).

660 63 McCulloch, J. A. *et al.* JAMS - A framework for the taxonomic and functional exploration of
661 microbiological genomic data. *bioRxiv* (2023).

662 64 Beghini, F. *et al.* Integrating taxonomic, functional, and strain-level profiling of diverse
663 microbial communities with bioBakery 3. *Elife* **10** (2021).

664 65 Wolock, S. L., Lopez, R. & Klein, A. M. Scrublet: Computational Identification of Cell
665 Doublets in Single-Cell Transcriptomic Data. *Cell Syst* **8**, 281-291 e289 (2019).

666 66 Wolf, F. A., Angerer, P. & Theis, F. J. SCANPY: large-scale single-cell gene expression data
667 analysis. *Genome Biol* **19**, 15 (2018).

668 67 Traag, V. A., Waltman, L. & van Eck, N. J. From Louvain to Leiden: guaranteeing well-
669 connected communities. *Sci Rep* **9**, 5233 (2019).

670 68 Aran, D. *et al.* Reference-based analysis of lung single-cell sequencing reveals a transitional
671 profibrotic macrophage. *Nat Immunol* **20**, 163-172 (2019).

672 69 Hao, Y. *et al.* Dictionary learning for integrative, multimodal and scalable single-cell
673 analysis. *Nat Biotechnol* **42**, 293-304 (2024).

674 70 Jin, S. *et al.* Inference and analysis of cell-cell communication using CellChat. *Nat Commun*
675 **12**, 1088 (2021).

676 71 Aibar, S. *et al.* SCENIC: single-cell regulatory network inference and clustering. *Nat Methods*
677 **14**, 1083-1086 (2017).

678 **Author contributions**

679 A.Z., R.H. and R.R.C. conceived and designed the study. R.R.C and R.H. supervised the
680 project. A.Z., R.H., Y.J., A.G., S.A., and C.E.M. performed experiments and collected
681 data. A.Z., J.H.B., Z.W., G.S., and V.N. performed computational analyses. S.H., H.N.S.,
682 J.W.L. and K.H. provided human microbiome samples, and S.K. and H.N.S. contributed
683 to clinical interpretation. X.X., M.J.M., Z.P., B.X. provided experimental input and
684 technical assistance. R.P. and N.M. provided technical expertise in bacteriology. J.H.B.,
685 Z.W., J.A.M., J.P.J. and C.O. contributed analytical tools, resources and expertise. A.Z.
686 and R.H. analyzed and interpreted data and prepared figures. A.Z., R.H. and R.R.C.
687 wrote and finalized the manuscript. All authors discussed the results, reviewed, and
688 approved the final manuscript.

689

690 **Acknowledgments**

691 We are grateful to NEI and NHLBI Flow Cytometry Cores, NEI Histology and Genetic
692 Engineering Cores, Ms. Wuxing Yuan, Dr. Shah Rashed and members of NCI Microbiome
693 Core, UCLA Goodman-Luskin Microbiome Center Microbiome Core, and all members of
694 the Caspi Lab for their invaluable experimental assistance. We extend special thanks to
695 Dr. Katsuko Sudo (Tokyo Medical University, Japan), Mr. Hirofumi Kobayashi and staff at
696 Sankyo Labo Service Corporation, Inc. (Japan), as well as the gnotobiotic management
697 team from NEI Veterinary Research and Resources Section for their expert support and
698 guidance in GF and gnotobiotic colony maintenance. We also thank Dr. Eduard Ansaldo
699 (NIAID) for sharing protocols for Akkermansia culture, Dr. Kikuji Itoh (Japan SLC, Inc.), Dr.
700 Koji Atarashi and members of the Honda Lab for providing experimental advice. Finally,
701 we acknowledge Dr. Geoffrey A. Mueller and staff at NIEHS Nuclear Magnetic Resonance
702 Group for their generous assistance with metabolomics, and Drs. Kelsey Wheeler, Daniel
703 Sellers, and Reuben Allen (Massachusetts Institute of Technology) for their insightful
704 discussions and critical feedback. This study was supported by NIH/NEI Intramural
705 funding, Project Number EY000184.

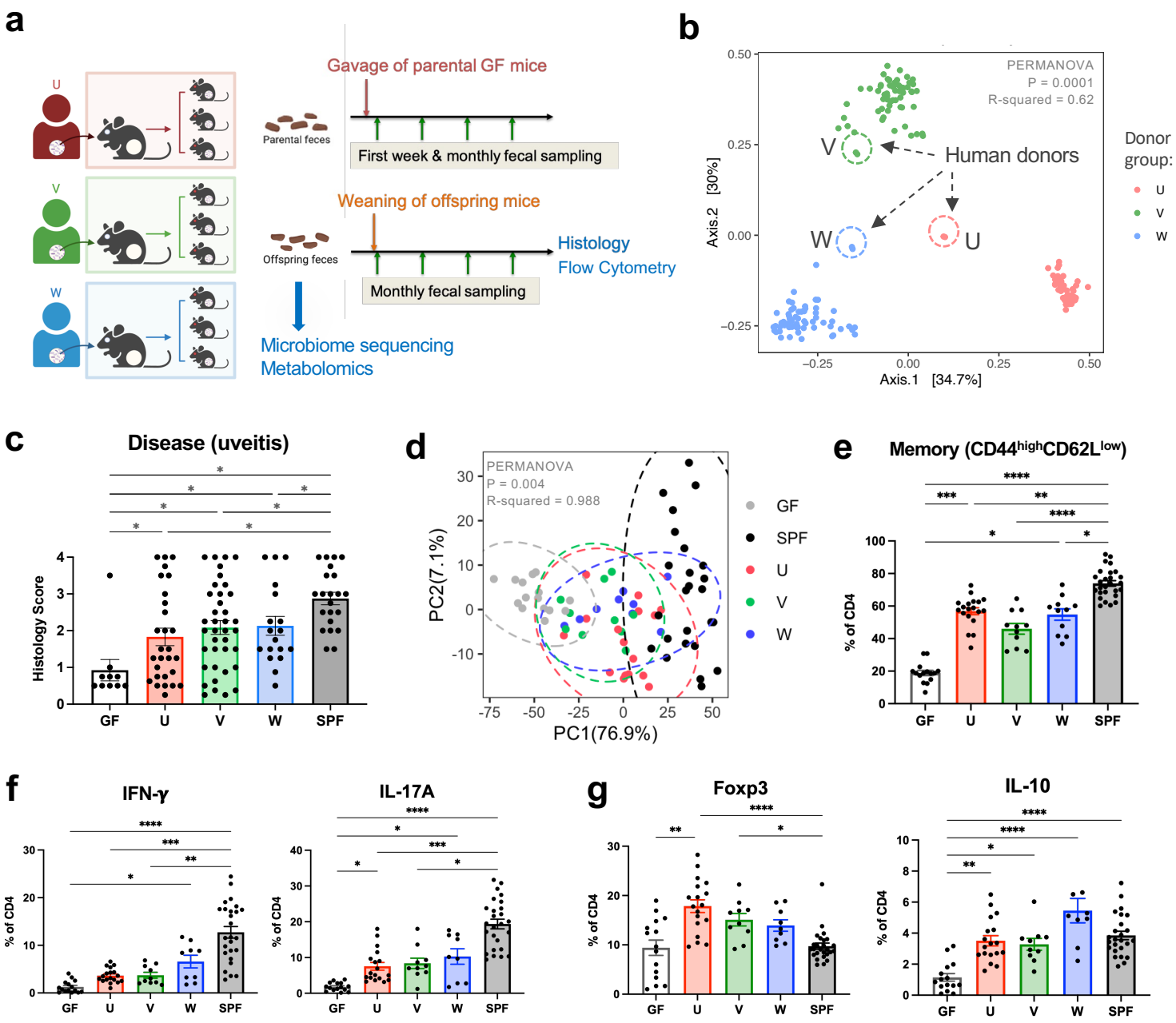

Fig. 1 | Human gut commensals support development of spontaneous experimental autoimmune uveitis (sEAU). a, Schematic representation of human fecal microbiota transfer experiments and data collection. **b**, Beta diversity based on Bray–Curtis dissimilarity showing differences in fecal microbiome composition between recipient groups U (n = 50), V (n = 59), W (n = 64). Encircled with dashed lines are the respective human donor (original) fecal samples. **c**, Disease scores (histology) of age-matched R161H mice (4-5 months old) from human flora (U, V, W, n = 28, 38, 18), SPF (n = 22) and GF (n = 10) groups (Kruskal–Wallis test between mouse recipient groups, p = 0.0002). **d**, Immunological clusters of CD4 T cells from colon lamina propria (LP) by the microbiome groups. PCA analysis performed on immune signature matrix by frequencies of CD4 T cells expressing each cell surface or intracellular marker (see **Extended Data Fig. 1e**). **e**–**g**, Frequencies of memory ($CD44^{high}CD62L^{low}$, **e**), IFN-γ- or IL-17A-producing (**f**), and regulatory (Foxp3-positive or IL-10-producing, **g**) CD4 T cells in colon LP of HuFl, SPF and GF R161H mice. **d**–**g**, Compiled data from 12 experiments, n = 15, 19, 11, 11, 27 for GF, U, V, W and SPF, respectively. Kruskal–Wallis tests show p < 0.0001 (**e**–**g**). P-values adjusted for post hoc multiple comparisons are displayed as asterisks. *P < 0.05, **P < 0.01, ***P < 0.001, ****P < 0.0001, and bar plots showing mean values ± SEMs (**c**, **e**–**g**).

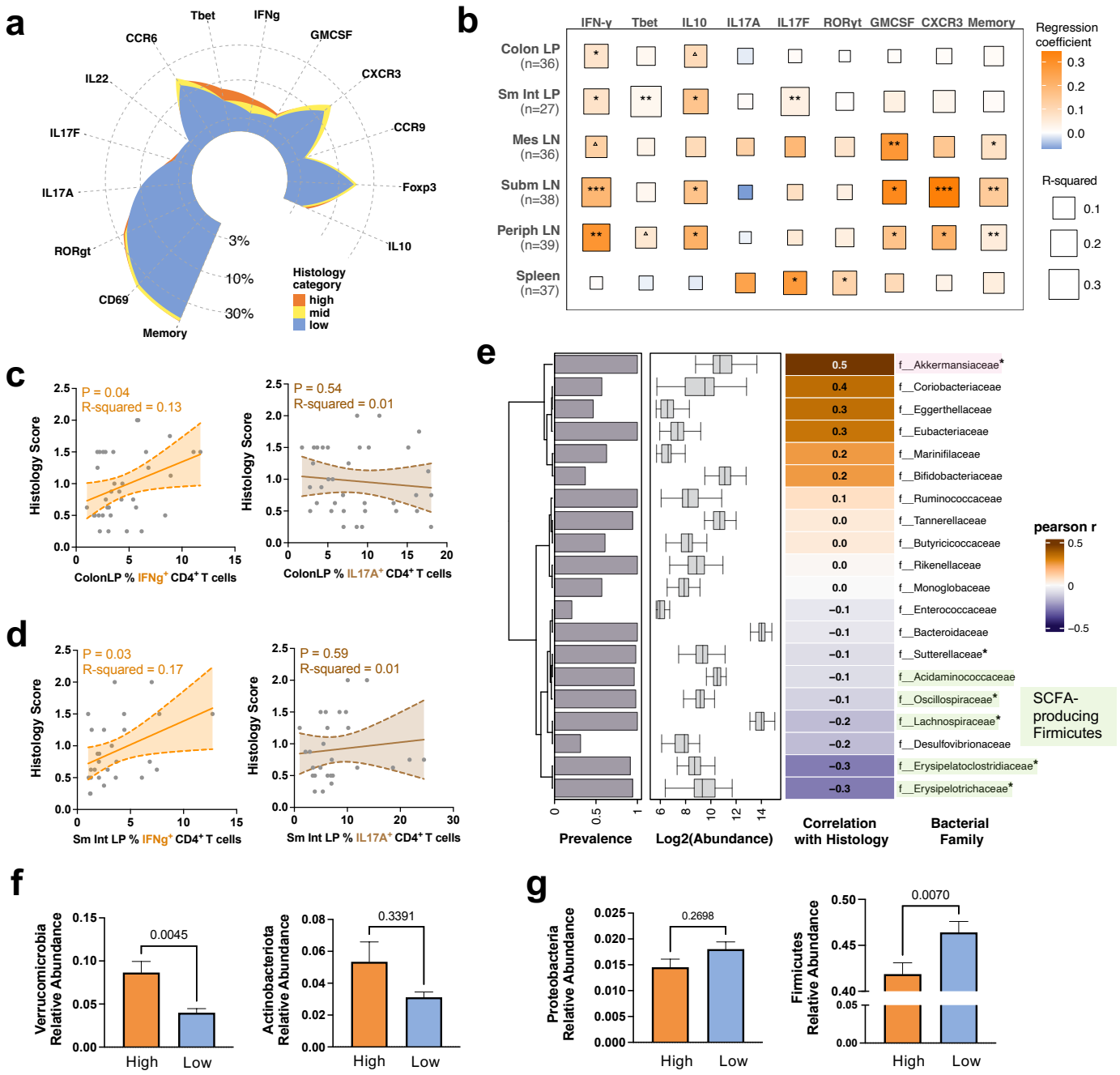

Fig. 2 | Human flora (HuFl) sEAU tracks with a dominant Th1 phenotype and abundance of Akkermansia (Verrucomicrobia). a, Mean relative frequency of colon LP CD4 T cells of each cell surface or intracellular marker arranged in a circular plot, colored by histology category: high (score ≥ 1.5, n = 10), mid (0.75 < score < 1.5, n = 8), low (score ≤ 0.75, n = 17). **b**, Correlational heatmap of histology scores with relative frequencies of each cell surface or intracellular marker in CD4 T cells across six tissue sites. LP, lamina propria; LN, lymph nodes; Sm Int, small intestine; Mes, mesenteric; Subm, submandibular; Periph, peripheral. $^{\Delta}$0.05 < P < 0.08, *P < 0.05, **P < 0.01, ***P < 0.001, modeled by simple linear regression. **c**–**d**, Representative trend lines with 95% confidence interval (shaded area) show that disease scores of HuFl mice are positively associated with IFN-γ-producing, but not IL-17A-producing, CD4 T cells, in colon LP (**c**) and small intestine LP (**d**). Data in **a**–**d** are aggregated from 8 experiments (UVW combined, sample sizes ranged from n = 27 to 39 across tissues following quality filtering). **e**, Correlational heatmap showing major fecal bacterial taxa (out of top 20 most abundant families) that correlate with disease scores in adult HuFl R161H (UVW combined, n = 105). P-values assessed after FDR (false discovery rate) correction following Pearson correlation. *P < 0.05. **f**–**g**, More Verrucomicrobia (**f**), and fewer Firmicutes (**g**) are present in the gut of HuFl mice with high disease scores. Sample sizes are n = 36 and 43 for high and low histology categories, respectively. Data in bar plots are presented as mean values ± SEMs, and P-values from Mann-Whitney U tests are shown in plots.

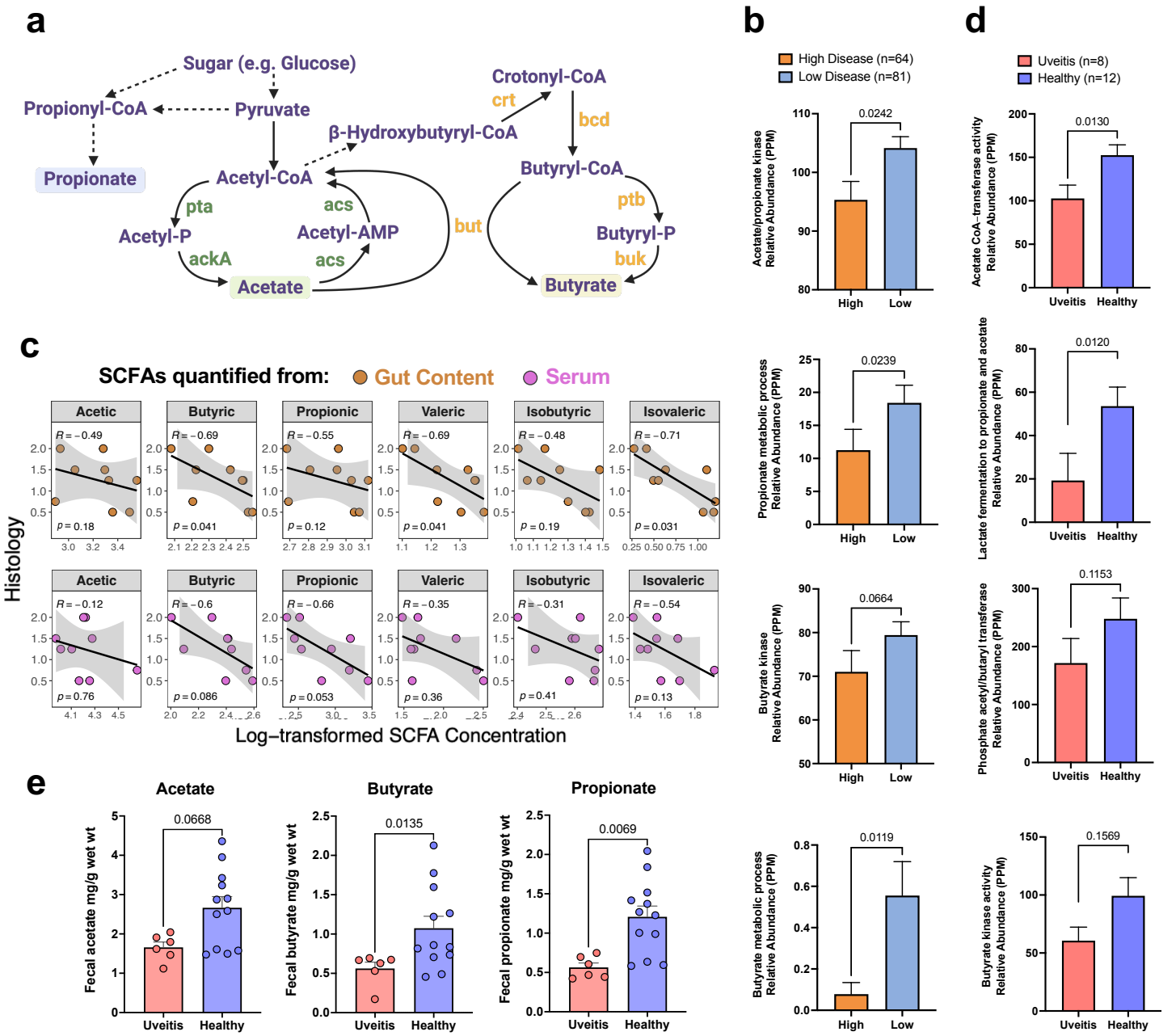

Fig. 3 | SCFA signatures are enriched in low disease HuFl mice or healthy subjects. a, A simplified pathway map highlighting functional genes involved in the main SCFA synthesis and metabolism. Dashed arrows indicate hidden intermediate steps. Abbreviations of enzyme symbols: pta, Phosphotransacetylase; ackA, Acetate kinase; acs, Acetyl-CoA synthetase; but, Butyryl-CoA:acetate CoA-transferase; ptb, Phosphate butyryltransferase; buk, Butyrate kinase; crt, Crotonase; bcd, Butyryl-CoA dehydrogenase. **b**, Enzymes in SCFA pathways (annotated with InterPro and Gene Ontology databases) are enriched in HuFl mouse gut with low histology scores (UVW combined, weanling and adult samples included). PPM, parts per million, a measure of relative abundance based on normalized base count for each feature in a metagenomic sample. **c**, Spearman correlation (visualized with a linear trend line) showing higher disease scores associated with lower SCFA concentrations both locally (in gut content) and systemically (in serum) in representative cohort U mice (n = 9). **d**, Enzymes in SCFA pathways (annotated with Gene Ontology and Pfam databases) are enriched in fecal samples from healthy humans compared to those from treatment-naïve uveitis patients, from a cohort of autoimmune uveitis (ocular-restricted, including idiopathic uveitis, VKH/SO and BCR). Sex, age, race and diet are comparably represented in patient and control groups. Normalized gene abundance is reported in PPM. **e**, SCFA levels from uveitis patients and healthy controls (same cohort as in **d,** but n = 6 available from the patient group). For **b, d** & **e**, Data are presented as mean values ± SEMs. Statistical significance was determined by Mann-Whitney U test.

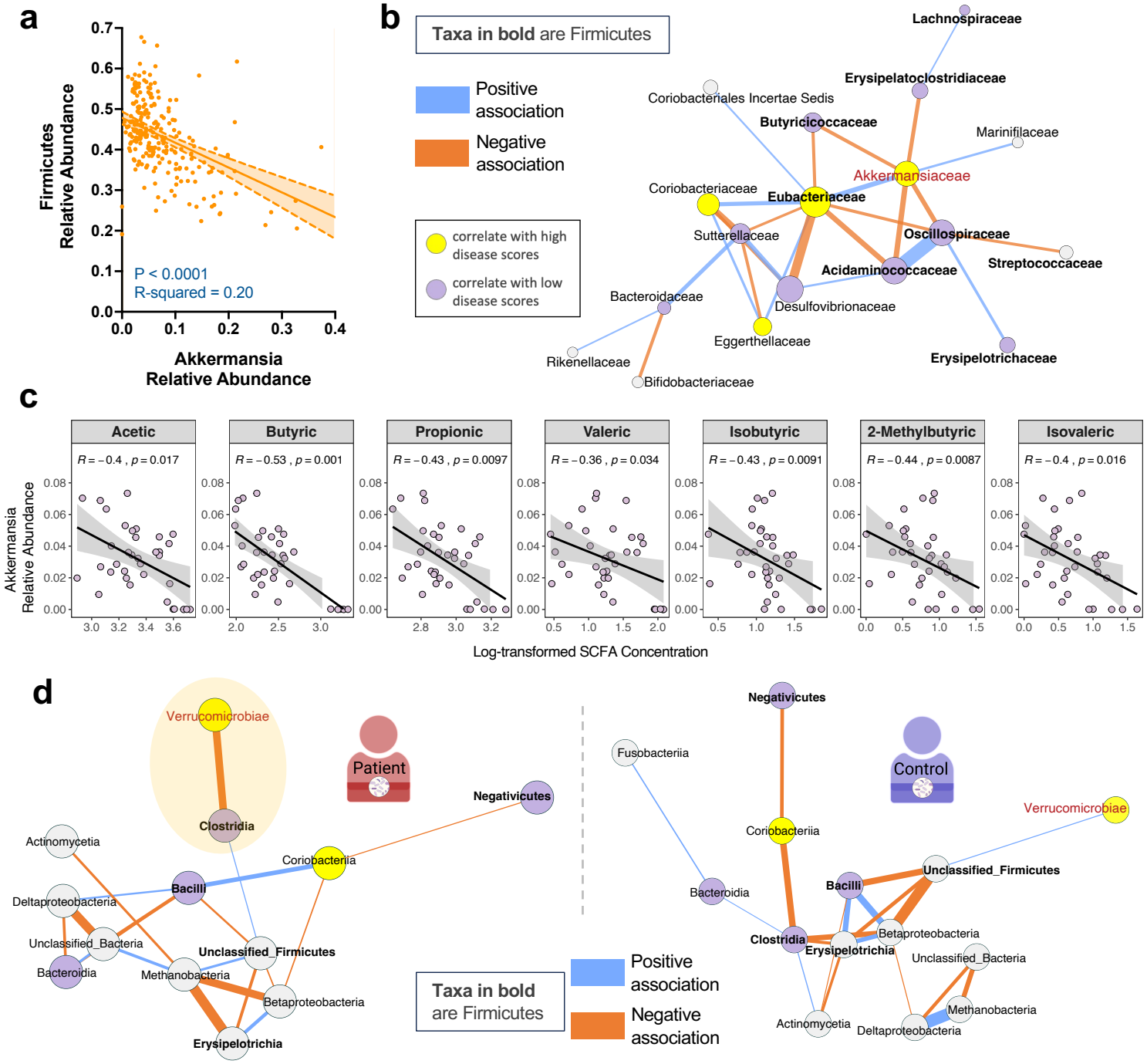

Fig. 4 | Akkermansia negatively correlates with Firmicutes in both sEAU and clinical uveitis. a, Simple linear regression showing a negative correlation of microbial relative abundance between Akkermansia (equivalent to Verrucomicrobia in this dataset) and Firmicutes in HuFl R161H mice (n = 234, UVW combined, weanling and adult samples included). **b**, Fecal bacterial association network exemplified in HuFl cohort V (n = 79, weanling and adult samples included). Network constructed at the taxonomic level of the bacterial family. Correlations with a threshold of Pearson r > 0.5 were transformed into dissimilarities via the "unsigned" distance metric, on which edge weights (strength of correlations) are based. Blue edges correspond to positive associations and orange edges to negative ones. Yellow and purple nodes represent taxa enriched in high *vs.* low disease categories, with Firmicutes labeled as bolded taxon names. Bigger nodes are more influential in the network (higher eigenvector centrality). **c**, Spearman correlation (visualized with a linear trend line) showing a negative association between relative Akkermansia abundance and SCFA concentrations in R161H gut (n = 35, UVW and SPF combined). Akkermansia was selected following multivariable association between SCFA concentrations and microbial features using MaAsLin2. **d**, Class level association networks in treatment-naïve uveitis patients (left, n = 8) and healthy controls (right , n = 12) from the same cohort of autoimmune uveitis. Correlations with a threshold of Pearson r > 0.3 are shown. Node and edge color schemes same as in **b**. Shaded ellipse in the patient network highlights the negative correlation between Verrucomicrobiae (Akkermansia) and Clostridia (Firmicutes), and this relationship is absent from the healthy human gut.

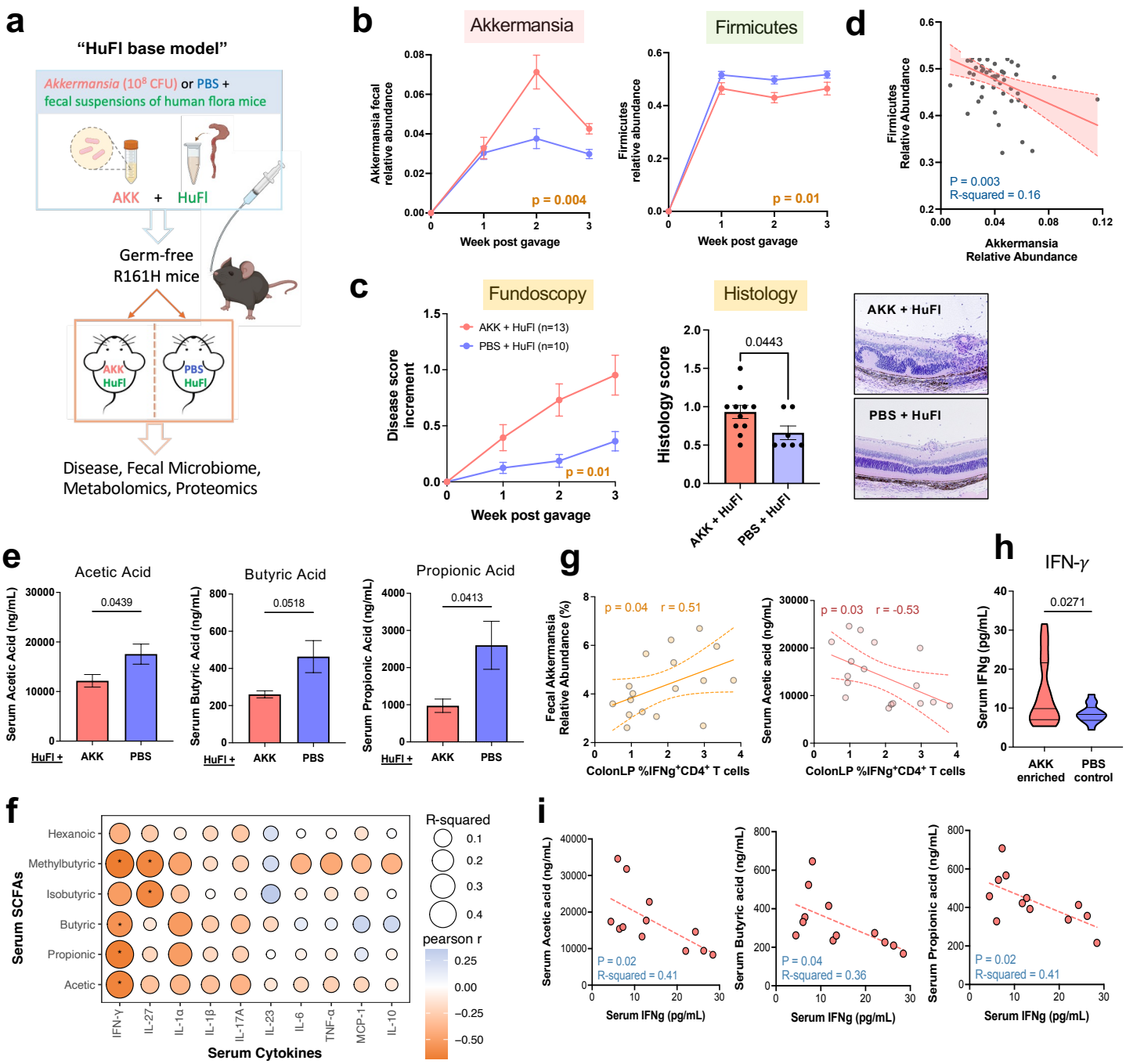

Fig. 5 | Akkermansia promotes uveitis by outcompeting SCFA producers and decreasing circulating SCFA levels. **a**, Study design of microbe reconstitution experiments. Previously GF R161H mice gavaged with a baseline human gut microbiota suspension (HuFl) plus *A. muciniphila* culture (AKK, 10^8 CFU) or sterile PBS. **b**, Relative abundance of Akkermansia and Firmicutes in feces from one representative of 3 experiments (n = 7 and 6 for Akk-rich and control, respectively). **c**, Left: Fundoscopy score increments from starting disease scores, combined from three experiments. Right: Histology scores and example images from 2 out of 3 experiments (n = 11 and 7 for Akk-rich and control, respectively). Mean values ± SEM. P-value determined by Welch-corrected t test. **d**, A negative correlation of relative abundance between Akkermansia and Firmicutes (n = 52, AKK and PBS groups combined, multiple time points included) by simple linear regression. **e**, Serum concentrations of main SCFAs are significantly lower in Akk-rich (n = 13) mice than in PBS controls (n = 10). Serum harvested 3 – 4 weeks post gavage, three experiments combined. **f**, Correlational heatmap of SCFA levels with cytokine concentrations in serum of engrafted mice. *P < 0.05, modeled by simple linear regression as well as Pearson correlation. **g**, Spearman correlation (visualized with a linear trend line) showing Akkermansia relative abundance associated positively, and serum acetic acid associated negatively, with the frequency of IFN-γ-producing CD4 T cells in colonic LP. **h**, Akk-enriched (n = 18) mice had higher serum IFN-γ concentrations compared to PBS control mice (n = 14), five experiments combined, of which two experiments used the minimal flora model. **i**, Representative trend lines show that main SCFA concentrations are negatively associated with IFN-γ levels in serum. Data in **g, i** are from 2 experiments (n = 12) using the minimal flora model.

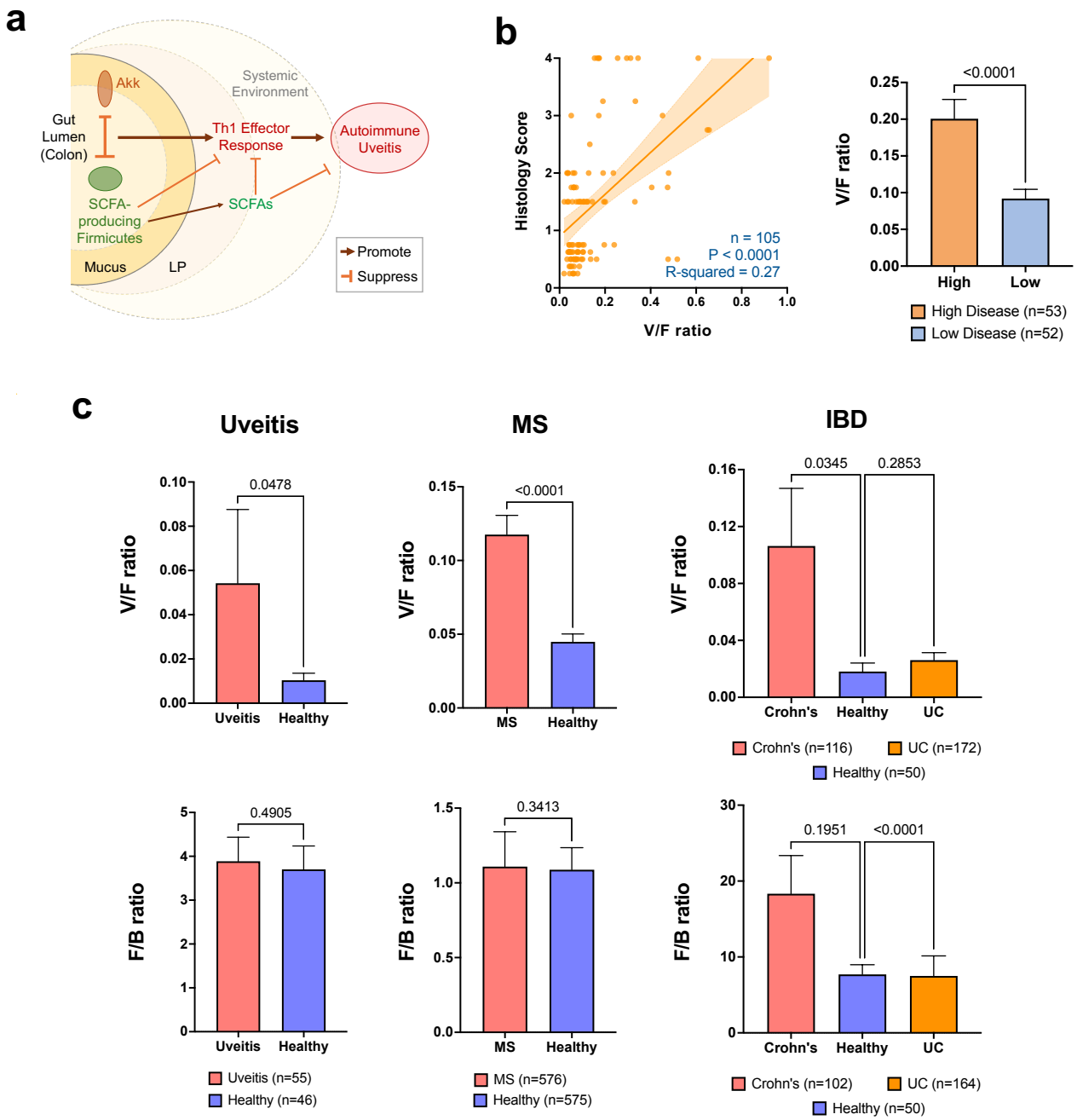

Fig. 6. **The inverse relationship between Verrucomicrobia and Firmicutes extends to clinical uveitis, multiple sclerosis (MS) and Crohn's disease. a**, Graphical summary of the working model. **b**, A positive correlation between V/F (Verrucomicrobia/Firmicutes) ratios and histology scores of HuFl mice by simple linear regression, and V/F ratios compared between high and low disease of HuFl mice. **c**, V/F and F/B (Firmicutes/ Bacteroidetes) ratios compared between patients from uveitis, MS and IBD and their respective healthy controls. Analyzed datasets of MS and IBD (Crohn's disease and UC) and healthy controls were from public sources. Uveitis and MS cohorts included those established on treatment. For F/B ratio in the IBD cohort, samples with <0.1% relative abundance of either Bacteroidetes or Firmicutes were removed from the analysis. Data are presented as mean values ± SEM. Statistical significance was determined by Mann-Whitney U test (one-tailed analysis was applied for uveitis and MS) and Kruskal–Wallis test with P-values adjusted for post hoc multiple comparisons (for IBD).